Wavelength-Selective $1 \times K$ Switches Using Free-Space Optics and MEMS Micromirrors: Theory, Design, and Implementation

Dan M. Marom, *Member, IEEE*, David T. Neilson, *Senior Member, IEEE, Member, OSA*, Dennis S. Greywall, Chien-Shing Pai, Nagesh R. Basavanhally, Vladimir A. Aksyuk, Daniel O. López, Flavio Pardo, Maria Elina Simon, Yee Low, Paul Kolodner, and Cristian A. Bolle

***Abstract*—The design and performance of several generations of wavelength-selective $1 \times K$ switches are reviewed. These optical subsystems combine the functionality of a demultiplexer, per-wavelength switch, and multiplexer in a single, low-loss unit. Free-space optics is utilized for spatially separating the constituent wavelength division multiplexing (WDM) channels as well as for space-division switching from an input optical fiber to one of K output fibers ($1 \times K$ functionality) on a channel-by-channel basis using a microelectromechanical system (MEMS) micromirror array. The switches are designed to provide wide and flat passbands for minimal signal distortion. They can also provide spectral equalization and channel blocking functionality, making them well suited for use in transparent WDM optical mesh networks.**

***Index Terms*—Gratings, microelectromechanical devices, microelectromechanical system (MEMS), optical add/drop multiplexing (OADM), optical filters, optical switches, wavelength-selective switch.**

I. Introduction

TRANSPARENT switching, where the optical signal does not undergo conversion to the electrical domain for switching purposes, can greatly simplify and reduce the cost of implementing optical networks by the elimination of optical to electrical to optical (OEO) conversions [1], [2]. The use of transparent switching within wavelength division multiplexed (WDM) systems further necessitates that switches be either wavelength-selective or be preceded by a demultiplexer and followed by a multiplexer for channel access [3]. The former is typically more desirable in many switching scenarios, since it avoids multiple components and will typically have lower losses and wider passbands. At an optical add/drop multiplexer (OADM) node, a subset of the optical channels, or wavelengths, propagating in the optical fiber is extracted for local detection (known as drop channels) and new optical channels are inserted in their place (known as add channels). The optical add/drop functionality can be achieved by the use of a channel blocking filter [4]–[6] placed between a passive splitter (for dropping channels) and a passive combiner (for adding channels). The device blocks the dropped channels from continuing to propagate in the line system and interfering with the added channels. A more efficient solution utilizes a wavelength-selective 2×2 switch [7], [8]. This switch has two inputs, the line system input, and the add channels and two outputs, the line system output, and the drop channels. These wavelength-selective switches use internal switching elements to route the individual WDM channels to the proper port.

As optical networks evolve from simple ring architecture with OADM nodes to optical mesh networks [1], the transparent switching requirements change. Mesh network nodes are typically linked to three or four neighboring nodes with each link carrying two-way traffic. Transparent switching at each node's network links, or cross connect functionality, is required for implementing an all-optical network. Furthermore, a modular cross connect fabric may be more desirable from an economic standpoint, as the node interconnecting links are deployed gradually. Finally, the cross connect may be required to support a power equalization feature [9] for optimal optical transport.

The wavelength-selective $1 \times K$ switch fulfills all the mesh networking requirements above [10]–[15]. The switch has a single input fiber that carries the WDM signal consisting of N channels, and distributes these N channels in a reconfigurable and independent fashion across the K output fibers. The switches [10]–[14] use a microelectromechanical system (MEMS) mirror array for the beam steering elements. Owing to the reciprocal nature of light propagation, the same switch fabric may be operated in reverse for wavelength-selective $K \times 1$ switching functionality. A complete wavelength-selective $K \times K$ cross connect (K WDM inputs and K WDM outputs) is implemented by utilizing K switch modules and K passive splitters [16]. A wavelength-selective $K \times K$ cross connect can also be constructed using blocking filters [5], [6], [17], but has additional loss since it requires both passive splitting and combining and further requires K^2 blocking filters component count.

In this paper, we review the technology of the wavelength-selective $1 \times K$ switch, from design choices and tradeoffs, through a description of various switch implementations we constructed, to the performance the switches exhibited.

Manuscript received June 7, 2004; revised January 7, 2005.

D. M. Marom and D. T. Neilson are with Bell Laboratories, Lucent Technologies, Holmdel, NJ 07733 USA (e-mail: dmarom@lucent.com).

D. S. Greywall, C. S. Pai, N. R. Basavanhally, V. A. Aksyuk, D. O. López, F. Pardo, M. E. Simon, Y. Low, P. Kolodner, and C. A. Bolle are with the Bell Laboratories, Murray Hill, NJ 09999 USA.

Digital Object Identifier 10.1109/JLT.2005.844213

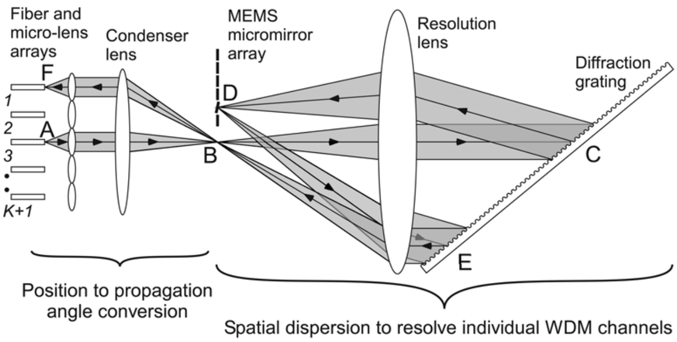

Fig. 1. Optical system configuration for wavelength-selective switch. The system is composed of a subsystem that converts fiber position to angle and a second subsystem, which uses a lens and diffraction grating to provide spatial dispersion to separate the channels.

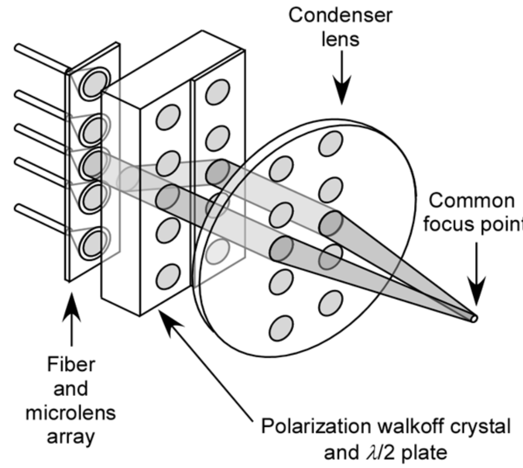

Fig. 2. Position to angle subsystem showing unequal spacing of fibers and lenses to introduce gaps for the variable attenuation function and polarization diversity optics.

II. Design of Wavelength-Selective $1 \times K$ Switches

The wavelength-selective $1\times K$ switch design is based on the guiding principle of optical imaging, leading to simple assembly and alignment. The optical system partitions the aperture to provide for multiple ports [7] and uses a coaxial relay imaging system to map the input beams onto the MEMS micromirror array and back. The coaxial arrangement facilitates assembly and packaging, as all elements are aligned along one-dimensional space, and can be housed in a robust tubular holder (symmetric structure with no weak bending axis). It is useful to consider the switch to be comprised of two major subassemblies (Fig. 1). The role of the first subassembly is to image the input and output optical fiber end faces onto a common magnified spot B. This subassembly converts the distinct spatial locations of the fibers to unique angular propagation directions at position B. A tilting mirror could be placed at this image plane to reflect the light and implement a nonwavelength-selective $1 \times K$ switch [18]. Here the light originating from the input fiber A would be imaged on the desired output fiber F. Attenuation level control can be obtained by deliberately misaligning the image location from the output fiber, by tilting this mirror away from the ideal coupling angle. The second subassembly introduces the desired wavelength-selectivity property. It spatially disperses the input magnified common spot, consisting of the N WDM channels, onto the MEMS micromirror array, such that each channel is imaged upon a separate mirror in the array for independent addressing. Each micromirror in the array is tilted to a desired angle, which determines the output fiber to which the reflected light will couple upon imaging back to the fiber array, on a WDM channel basis. A typical beam path in the switch originates from the input fiber A and is imaged with magnification to B by the first subassembly. The second subassembly images one of the WDM channels from B to D, according to wavelength. The micromirror at D is tilted to a prescribed angle, and the reflected light that is propagating in a new direction is imaged back to point B by the second subassembly. Finally, the first subassembly images the reflected signal to the output fiber location F by a last imaging operation.

Due to the independent imaging operations each subassembly performs, we may analyze the operation of each subassembly independently. The first subassembly determines the magnification ratio, the fiber array layout, and the required mirror tilts to reach each output fiber. The second subassembly determines the amount of spatial dispersion for separating the WDM channels and obtaining the necessary passband width. We will establish the characteristics of each subassembly, as well as the overall design tradeoffs of the wavelength-selective switch.

A. Position-to-Propagation Angle Subassembly

The optical subassembly responsible for imaging the optical fiber end faces onto a common magnified spot is comprised of a fiber array, a matching microlens array, polarization diversity optics, and a condenser lens whose aperture subtends all the beam apertures from the fibers (Fig. 2). The fiber array consists of $K+1$ fibers, where one fiber is assigned to carry the input signal, and the remaining K fibers are the output fibers. The optical axes of the individual lenses and fibers are coaxially aligned and arranged in a one-dimensional array to accommodate mirrors with a single tilt axis. Furthermore, the fibers and lenses are placed on an irregularly spaced grid to introduce gaps between some of the lens apertures. This supports the attenuation function without giving rise to crosstalk. We also employ a polarization-diversity solution to eliminate the polarization sensitivity of the diffraction grating employed in the second optical subassembly. The polarization diversity is provided by an anisotropic uniaxial crystal and a half-wave plate. The uniaxial crystal separates an input beam into two distinct (non overlapping), copropagating, orthogonally polarized beams. The half-wave plate rotates the polarization state of one of the beams such that the two beams are copolarized. The two beams propagate within the optical subsystem, and are merged back to a single-beam before coupling to the selected output fiber by the waveplate and uniaxial crystal combination. Due to the imaging operation, the two beams exchange their positions in the return path toward the output fibers. Thus, path length differences between the two beams, as experienced by the beam traversing the half-wave plate, are compensated in the return path. This ensures that the system will also have low polarization mode dispersion (PMD).

The optical arrangement of the first subassembly implements a telescopic imaging system via the lenses from the microlens array (focal length f_1) and the condenser lens (focal length f_2). The imaging operation magnifies the optical beam emerging from the single mode fiber by factor $M = f_2/f_1$. The $F\#$ of the lenses in the microlens array are matched to the optical beam's numerical aperture (NA). Using a Gaussian beam waist of 10.5 μm for the beam from a single-mode fiber, the lens $F\#$ should be at most 3.5 to prevent significant beam clipping ($< 1\%$). It is desirable to pack the microlenses in the lens array as tightly as possible, to keep the $F\#$ of the condenser lens as large as possible. At minimum, the microlens pitch will equal the individual lens diameter, D_L, and the condenser lens aperture is, therefore, $D_L(K+1)$. However, for implementing the spectral equalization functionality, increased spacing between microlenses is required to allow for attenuation by beam displacement for intentional imperfect coupling to the output fiber. To conserve the condenser lens aperture, the intermicrolens spacing, or gaps, are inserted between every pair of microlenses. This ensures that there is a gap available to only one side of each microlens in the array for attenuation by beam displacement, and a total of $K \div 2$ gaps, where the symbol $\div$ denotes the div operation.

The intermicrolens spacing, or gap size, is determined from the required attenuation dynamic range and minimum crosstalk requirements. At the maximal attenuation setting required, we must still suppress the crosstalk to the adjacent output fiber. We define the microlens pitch at locations where a gap is inserted as P_L (Fig. 3). The gap size is, therefore, $P_L - D_L$. For a given beam shift x_0 from the microlens optical axis, the attenuation to the desired output fiber and the crosstalk to the neighboring fiber is calculated by the power overlap integral [19], yielding

$$\eta_{\text{attenuation}}(x_0) = \left| \int_{\text{lens aperture}} \Psi(x,y)\Psi(x-x_0,y)\,dxdy \right|^2 \quad (1)$$

and

$$\eta_{\text{crosstalk}}(x_0) = \left| \int_{\text{lens aperture}} \Psi(x,y)\Psi(x+P_L-x_0,y)\,dxdy \right|^2 \quad (2)$$

where the collimated beam profile is denoted by $\Psi(x,y)$. Note that the finite extent of the microlens aperture assists in the attenuation functionality, as a fraction of the beam power is lost. In our designs, the criteria are for 10-dB attenuation range while maintaining crosstalk below 40 dB. Using a Gaussian beam approximation for the beam profile and microlenses of $F\# = 3.5$, then the necessary pitch P_L is approximately 1.5 times the lens diameter D_L (or gap size is one half the lens diameter).

The condenser lens aperture with added gaps of half diameter size is, therefore, $D_L(K+1) + (D_L/2)(K \div 2)$. Given the condenser lens aperture and focal length, we can now evaluate its $F\#$ as

$$F\#_{\text{cond}} = \frac{F\#_{\mu\text{lens}} M}{\frac{K+1+(K\div 2)}{2}} \approx \frac{F\#_{\mu\text{lens}} M}{\frac{5K}{4+1}}. \quad (3)$$

The condenser lens $F\#$ decreases as the magnification factor M decreases and as the number of output fibers K increases. If there is no need to support the spectral equalization functionality, no gaps are required, and the denominator of (3) simplifies to $K+1$. Since K is determined by the required functionality, the only free parameter available for the designer is the magnification factor. A high magnification factor would be desirable for implementing the condenser lens. This would also reduce the mirror tilt angle ranges. If the input fiber is in the middle of the fiber array, as in Figs. 1 and 3, then the mirror must tilt roughly within the range $\pm 1/(4F\#_{\text{cond}})$, in radians. Alternatively, the input fiber may be at the edge of the array, requiring the mirror to tilt in only one direction but at a doubled range of $1/(2F\#_{\text{cond}})$. However, as the magnification ratio M increases, the resulting mode size at the output of the first subassembly also increases. This places a burden on the second subassembly responsible for the spectral resolution, as described in Section II-B.

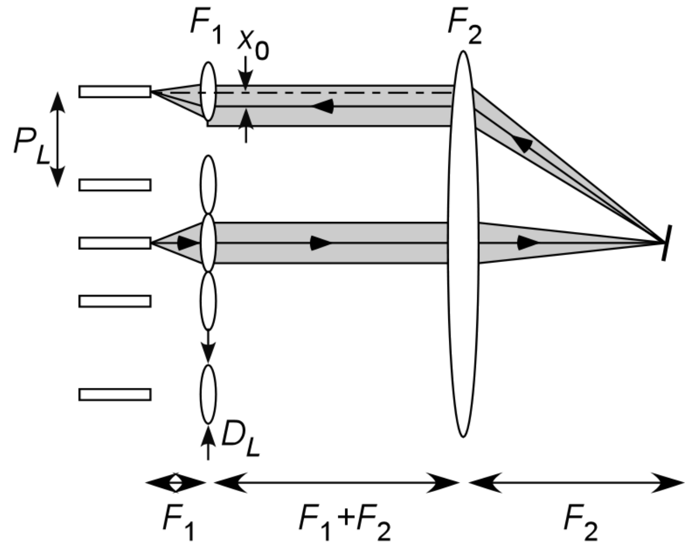

Fig. 3. Position-to-angle conversion optics showing configuration of optics for providing variable attenuation function while maintaining maximum density. The displacement of the beam x_0 causes attenuation by changing the coupling angle at the fiber.

B. Spatial Dispersion Subassembly

The second optical subassembly spatially disperses the magnified mode that was generated by the first subassembly and images it on the micromirror array. Its design is similar to a spectrometer with a Littrow mounted grating. A single lens collimates the light that is then incident on the grating. The diffracted light, which is propagating back toward the lens and is angularly dispersed, is imaged by the same lens onto the micromirror array. As is well known from classical spectrography, the spectral resolution of the instrument increases with increasing focal length and grating frequency, and with decreasing input slit size. In our switch, the magnified mode size is equivalent to a spectrograph slit size. Therefore, it is desirable to minimize the spot size (decrease M) for obtaining high spectral resolution.

The spatial dispersion, expressed in meters per hertz, provided by the second subassembly is given by [20]

$$\frac{dx}{d\nu} = \frac{2\lambda_0 f_3 \tan(\phi)}{c} \quad (4)$$

where λ_0 is the center wavelength of the WDM system, f_3 is the focal length of the resolution lens, c is the speed of light, and ϕ is

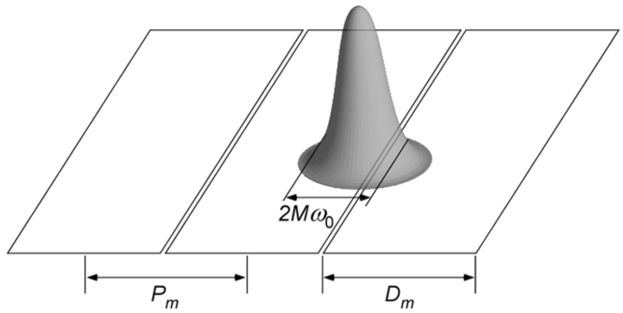

Fig. 4. Schematic of magnified Gaussian mode at a single frequency component imaged on the mirrors of width D_m and pitch P_m. Mode size is M times larger than the output of a single mode fiber, $2\omega_0$, where M is the magnification factor of the imaging system.

the Littrow grating mounting angle. The Littrow angle is given by $\sin(\phi) = \lambda_0\nu_g/2$, where ν_g is the grating spatial frequency (in m^{-1}). Therefore, the mirror pitch of the micromirror array will be $P_m = \nu_{\mathrm{ch}} \cdot dx/d\nu$, where ν_{ch} is the WDM channel frequency spacing (in Hz). Note that we are assuming constant spatial dispersion across the total bandwidth of the optical system. In reality, especially for gratings of high spatial frequency, the mirror pitch will not be constant due to the wavelength dependence in the grating diffraction formula [20].

The spatially dispersed image of the magnified Gaussian mode, Fig. 4, present on the micromirror array can be expressed as

$$\varphi(x,y,\nu) = \sqrt{\frac{2}{\pi M^2\omega_0^2}} \exp\left[-\frac{\left(\frac{x-P_m\nu}{\nu_{\mathrm{ch}}}\right)^2 + y^2}{(M\omega_0)^2}\right] \quad (5)$$

where ω_0 is the Gaussian mode field radius of the beam from a single mode fiber (5.25 μm). The term $P_m\nu/\nu_{\mathrm{ch}}$ in (5) defines the center location of the magnified Gaussian mode as a function of the temporal frequency. The dimensionless ratio ξ of mirror size to the magnified Gaussian mode size $\xi = P_m/(M2\omega_0)$ measures how well the Gaussian mode is confined within the micromirror, and will be shown to determine the passband performance. The frequency-dependent, power-coupling efficiency integral is calculated by performing the traditional overlap integral over the extent of a single mirror at the device plane [19]. More elaborate modeling taking into account the effect of the neighboring mirror states has been performed elsewhere [21]. With the simple model, the coupling efficiency is defined by

$$\begin{aligned}\eta(\nu) &= \left|\int_{y=-\infty}^{\infty}\int_{x=-D_m/2}^{D_m/2} \varphi(x,y,\nu)^2 dx dy\right|^2 \\ &= \frac{1}{4}\left\{\mathrm{erf}\left[\sqrt{2}\xi\left(\frac{D_m}{P_m} - \frac{2\nu}{\nu_{\mathrm{ch}}}\right)\right]\right. \\ &\qquad \left. + \mathrm{erf}\left[\sqrt{2}\xi\left(\frac{D_m}{P_m} + \frac{2\nu}{\nu_{\mathrm{ch}}}\right)\right]\right\}^2 \end{aligned} \quad (6)$$

where D_m is the physical width of the micromirror in the spatial dispersion direction, and the mirror is modeled as infinite in the orthogonal direction. The mirror size D_m is slightly smaller than the mirror pitch P_m, due to the presence of a gap to prevent physical contact between adjacent mirrors. We can derive simple expressions for the passband and stopband widths of a WDM channel using (6) with the approximation that the contribution of the second error function is constant, which is valid when designing for flat and wide passbands. The passband width ν_{pass} normalized by the channel spacing and measured at η transmissivity level (a characteristic level is $\eta = 0.5$ or -3 dB passband) is defined by

$$\frac{\nu_{\mathrm{pass}}}{\nu_{\mathrm{ch}}} \cong \frac{D_m}{P_m} - \frac{1}{\sqrt{2}\xi}\mathrm{erf}^{-1}\left[\sqrt{4\eta} - 1\right] \quad (7)$$

where erf^{-1} is the inverse error function. Similarly, the stopband width ν_{block}, originating from crosstalk of neighboring mirrors (or adjacent channels) is

$$\frac{\nu_{\mathrm{block}}}{\nu_{\mathrm{ch}}} \cong 2 - \frac{D_m}{P_m} - \frac{1}{\sqrt{2}\xi}\mathrm{erf}^{-1}\left[1 - \sqrt{4\eta}\right]. \quad (8)$$

The stopband width is typically measured at the $\eta = 10^{-4}$ $(-40\ \mathrm{dB})$ level. The two parameters influencing the passband and stopband widths are the fill factor of the array D_m/P_m and the confinement ratio ξ. It is desirable to maximize both bandwidths for minimal signal distortion and crosstalk, which can be satisfied by an increasing confinement ratio ξ. A high fill-factor micromirror array also maximizes the passband width, yet decreases the stopband width. Nevertheless, the mirror arrays are typically fabricated with minimal gap size as technically feasible for maximizing the passband width. In the limiting case of $D_m \to P_m$, the fill-factor approaches 1 and the confinement parameter ξ is the only parameter determining the passband shape, controlling the extent of the passband flatness and the roll-off rate (Fig. 5). Thus, passband requirements can be accommodated by varying the ratio of the mirror size to the magnified Gaussian mode size, which sets ξ.

The available degrees of freedom remaining in designing the second optical subassembly is choice of diffraction grating and lens focal length. For obtaining high spectral resolution within a small package, it is always desirable to select a high spatial frequency diffraction grating. Other factors influencing the grating selection process are the diffraction efficiency and polarization dependence in the telecom (1500–1620 nm) wavelength range. We employ polarization diversity in our switch, implemented in the first subassembly, as the chosen grating does have significant polarization dependence. Once the magnification factor and diffraction grating have been selected, the focal length f_3 of the resolution lens can be established to meet the passband performance metrics. The lens's $F\#$ is equal to the condenser's, as evaluated by (3). However, this lens has a field of view diameter determined by the physical extent of the micromirror array, or $N \cdot P_m$. These two requirements, combined with the spectral range, imply that the resolution lens will require multiple elements to obtain good imaging characteristics, and warrant a custom design.

As outlined above, the design process of a wavelength-selective $1 \times K$ switch is straightforward. Given the switch requirements (number of output fibers, spectral equalization dynamic range, and channel passband characteristics), the optical parameters are established. The designer can vary the magnification factor M, which will affect the lenses' $F\#$, overall system size,

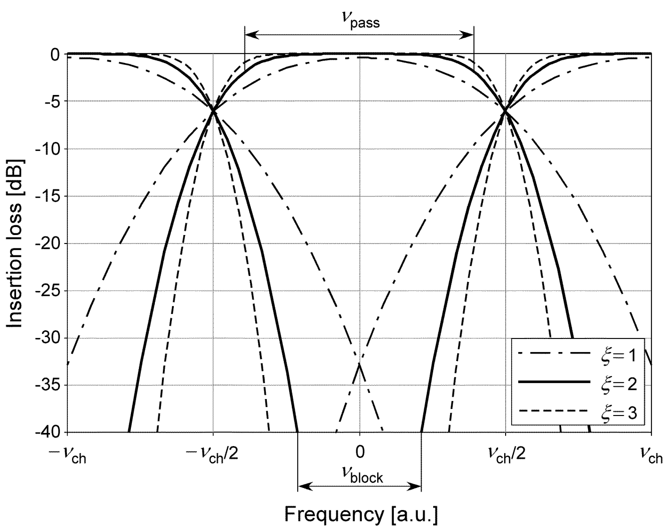

Fig. 5. Calculated passbands as a function of the confinement parameter ξ. Assumes a 100% fill-factor micromirror array, and effect of neighboring mirror is neglected. ξ is the ratio of mirror size to beam size and $\nu_{\rm ch}$ is the channel-to-channel frequency spacing.

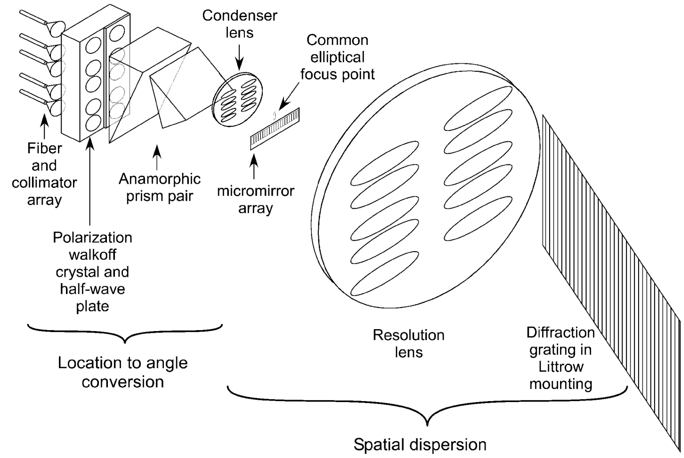

Fig. 6. Schematic of optical system showing the effect on beam size and shape of inserting anamorphic optics. The anamorphic optics ensures that high spectral resolution can be maintained while the apertures of the optics are minimized.

and micromirror scan range, and confinement factor ξ, until a suitable design space is achieved. However, having so few critical parameters influencing the switch design is often too restrictive. We introduce anamorphic optics to obtain an additional design parameter that may lead to more efficient switch implementations.

C. Anamorphic Optics

The use of free-space optics in our switch design allows us to better utilize the three-dimensional volume of the switch package. We observe that the lenses' $F\#$ is determined by the extent of the linear array of $K+1$ beam apertures. In addition, the spectral resolution is determined by the magnified Gaussian beam width in the dispersion direction only. We introduce anamorphic optics to convert the circular Gaussian beam profiles to elliptical ones. The anamorphic optical elements are inserted into the first optical subassembly to generate a magnified elliptical beam whose narrow axis is in the spatial dispersion direction of the second optical subassembly. This ellipse orientation continues to satisfy the minimal beam size requirement for the spectral resolution.

The anamorphic elements are placed between the microlens array and the condenser lens, in the collimated beam region, and serve to compress the beams' vertical dimension by factor R. The fiber and microlens arrays are also both oriented vertically when employing the anamorphic optics (Fig. 6). Orienting the fiber array vertically means that the MEMS mirrors must tilt about an axis parallel to the dispersion direction. This is desirable for maximizing the channel passband [21] and reducing the sensitivity to mirror curvature [22]. The anamorphic effect reduces the extent of the $K+1$ beam apertures by R, increasing the condenser lens $F\#$ to

$$F\#_{\rm cond} \approx \frac{F\#_{\mu{\rm lens}} M R}{\frac{5K}{4+1}}. \tag{9}$$

The benefit further extends to the $F\#$ of the resolution lens, as well as to the micromirror scan range, without effecting the confinement factor ξ. Therefore, we can now modify three parameters in order to reach a desirable switch design; the magnification ratio M and confinement ration ξ for determining the spectral resolution, and the anamorphic ratio R for controlling the lenses' $F\#$.

The advantages listed above may lead to a conclusion that the use of anamorphic optics is purely beneficial. However, the magnified elliptical beam requires the mirrors in the micromirror array to be longer by factor R. This can make the design of the MEMS mirrors more difficult since they are now longer in the direction of tilt, will have greater mass, and be more susceptible to curvature. Furthermore, the mirror resolution in tilt angle is also finer, requiring greater precision in mirror positioning.

III. Implementation of Wavelength-Selective $1 \times K$ Switches

We have realized three successful generations of wavelength-selective $1 \times K$ switches. These switches were designed to support the switching functionality, and provide wide and flat passbands for minimal signal filtering. Filtering is particularly critical since it is expected that signals will pass through multiple switches, and concatenated filtering will narrow the system passband [17], [23].

Common to all our switches is the support of a WDM system operating at the extended L-band (1554–1608 nm). Low insertion losses were achieved by using an 1100 lines/mm grating with high diffraction efficiency in the grating's S-plane [24] (polarization perpendicular to the groove direction), along with the aforementioned polarization diversity. The grating was Littrow-mounted at angle $\phi = 60.5^\circ$ (angle for center wavelength $\lambda_0 \sim 1582$ nm). The two logical subassemblies describe above were implemented as physical subassemblies, since this made building various optical configurations more practical. Particular description of each switch version is provided below.

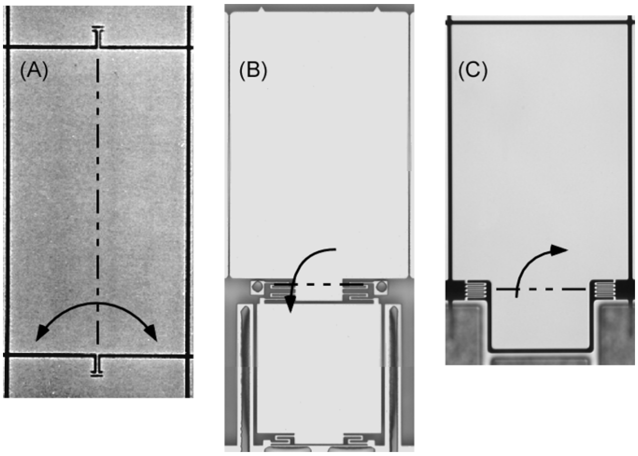

Fig. 7. Electrostatically actuated MEMS mirrors for wavelength-selective switches (one micromirror of high-fill-factor array shown). A torsional mirror with a rotation axis orthogonal to the dispersion direction is shown in (A). Both mirrors in (B) and (C) tilt about an axis parallel to the disperion direction. The design in (B) uses a double hinged actuator while that in (C) is fringing-field actuated.

A. 128-Channel 1 $\times$ 4 Wavelength-Selective Switch

Our first generation wavelength-selective switch was configured with a single input and four output fibers. The switch supported 128 channels spaced on a 50-GHz grid, and was designed to provide channel bandwidth support of 10-Gb/s transmission rates.

The first optical subassembly implemented an imaging system with magnification of $M = 3.3$. No anamorphic optics were used. The five fibers and lenses were tightly packed, as this switch was not designed to support dynamic spectral equalization. Using (3) with a correction to the denominator due to the tight lens packing, the theoretical condenser lens $F\#$ is $\sim$ 2.3. In practice, an $F\#$ of 2 was required, due to the increased aperture requirement for the polarization diversity. The input fiber was placed at the center of the array, requiring a micromirror tilt range of $\pm 5.6^\circ$. A five-element, 100-mm focal-length resolution lens was designed for the second optical subassembly with the prescribed aperture and field diameter. The lens and grating combination provide a spatial dispersion of 1.86 μm/GHz, resulting in a micromirror pitch of 93 μm, and the entire array was $\sim$ 12-mm long. In practice, the mirror pitch varied from 82 to 108 μm due to the nonlinearity in the grating's angular dispersion. The resolution lens focal length was chosen to provide a confinement ratio of $\xi = 2.7$.

The switch employed a MEMS mirror array, with the mirrors tilting in the direction of the spatial dispersion [Fig. 7(a)]. The MEMS mirrors were etched in a 1-μm-thick silicon-on-insulator (SOI) wafer and had two 0.5-μm-thick torsion rods defining their rotation axis. The SOI mirror chip was flip-chip-bonded onto an electrode chip with a 10-μm spacer. The mirrors were actuated by an electrostatic attractive force imposed by one of two electrodes below each mirror on either side of the axis. These MEMS micromirrors were designed to rotate up to $\pm 8^\circ$, at a voltage of $\sim$ 200 V dc applied to either mirror electrode. A 2-μm gap between the mirrors provided a 98% fill-factor for the array in the spatial dispersion direction.

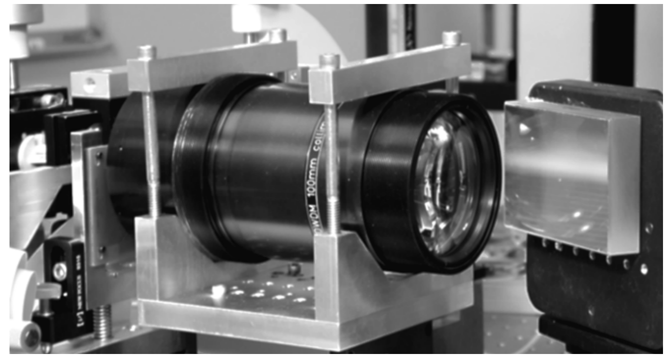

Fig. 8. Picture of the assembled 128-channel 50-GHz channel spacing 1 $\times$ 4 wavelength-selective switch. The 100-mm focal length lens is in the center with the 1100-lines/mm grating to the right.

The switch prototype was assembled on an optical table (Fig. 8). The length of the optical system was $\sim$ 350 mm.

B. 64-Channel 1 $\times$ 2 Wavelength-Selective Switch With Spectral Equalization

Our second-generation wavelength-selective switch was configured with single-input and two-output fibers. The switch supported 64 channels spaced on a 100-GHz grid, and was designed to provide channel bandwidth support of 40-Gb/s transmission rates.

One key objective set for the design of the switch was to reduce its physical size. This was achieved primarily by reducing the focal length of the resolution lens to 50 mm. However, the spectral dispersion of the second subassembly was halved to 0.93 μm/GHz by this action. Since the channel spacing was doubled to 100 GHz, the micromirror pitch remained at 93 μm, and the entire array was $\sim$ 6-mm long. The requisite channel passbands were achieved by increasing the confinement ratio to $\xi = 3.2$, implying a reduction in the magnification ratio to $M = 2.75$. The lenses' $F\#$ was maintained sufficiently high by using one of the fibers both as an input and an output through the use of an optical circulator. Thus, the switch utilized only two fibers, resulting in a reduced aperture requirement. Using (3) with a value of $K = 1$ yields a theoretical $F\#$ of 4.2, but was 2.6 in practice due to the polarization diversity. The first optical subassembly utilized a dual-fiber collimator (two fibers placed at the lens' front focal plane), followed by an adjustment prism to maintain parallelism for the two collimated beams. The prism was placed at a location that defined the necessary beam separation to provide for the spectral equalization functionality. The micromirrors were required to tilt in the direction orthogonal to dispersion, in support of the spectral equalization functionality. To reduce the electrical I/O requirements, the mirrors utilized single-sided actuation (one electrode per mirror). The mirror tilt range was, therefore, $1/2F\#$, or $\sim 7^\circ$ (using theoretical $F\#$ value of 4.2). A four-element, 50-mm resolution lens was designed for the second optical subassembly.

Two different MEMS micromirror arrays were designed for the switch; one based on surface micromachining of polysilicon and the other on bulk processing of a SOI wafer [25], [26]. In the polysilicon approach, a double-hinge activation mechanism is defined. An actuation plate, anchored at one edge, is tilted to small angles via an underlying parallel plate electrode and

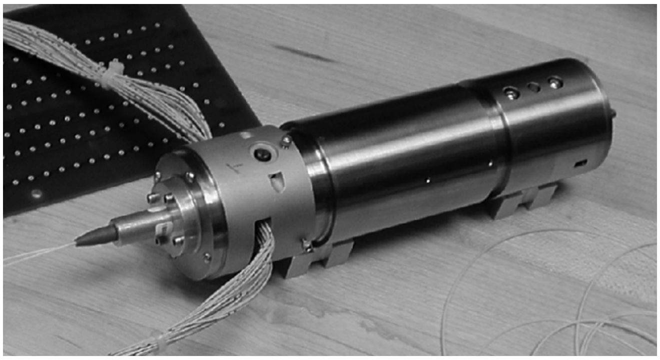

Fig. 9. Picture of an assembled 64-channel 1×2 wavelength-selective switch with spectral equalization. The housing is 190-mm long and 44-mm outer diameter.

a 4-μm gap. The mirror is attached to the free edge of the actuation plate and to the substrate with unequal arm lengths, allowing large mirror tilt angles out-of-plane via angle amplification [Fig. 7(b)]. The mirror, actuator plate, and springs are etched in the 1.5-μm-thick polysilicon. Spring features are typically 0.5-μm wide, and the gap between adjacent mirrors is 0.7 μm ($\sim$ 99% fill ratio). In the SOI approach, a 10-μm layer of polysilicon is deposited over the patterned 1-μm-thick single-crystalline silicon and is used to define the actuator electrodes and ground shields. The electrode attracts the short actuator arm via an electrostatic fringing field, resulting in mirror rotation out-of-plane about the torsion springs [Fig. 7(c)]. The monolithic structure does not exhibit rotational snap-down.

As shown in Fig. 9, the switch was packaged in a Super-Invar tube to make it insensitive to temperature variations. The tube size was 44-mm outer diameter $\times$ 190-mm length, and it weighed 1.25 Kg.

C. 64-Channel 4 × 1 Wavelength-Selective Switch With Spectral Equalization and Anamorphic Optics

Our third-generation wavelength-selective switch was configured with four input fibers and a single output fiber (the switch is physically identical to a 1×4, as the optical path is reciprocal). This configuration is most appropriate for implementing cross connect functionality among four WDM systems with broadcast capability and hitless switching [16]. This switch, also supported 64 channels spaced on a 100-GHz grid, and was designed to provide channel bandwidth support of 40-Gb/s transmission rates.

The form factor and spectral resolution optics of our second-generation switch were preserved in this new five-fiber switch, which is shown in Fig. 10. Anamorphic optics was, therefore, added in the first subassembly to support the higher fiber count without changing the resolution lens' $F\#$. The fiber and matching lens array were irregularly spaced to support the spectral equalization functionality (two gaps of half lens diameter inserted in arrays). The anamorphic ratio was $R = 3$, which was achieved with a prism pair. The magnification ratio was $M = 2.5$. The chosen parameters lead to the lenses' $F\# = 4.3$, which reduced to 2.8 on account of the polarization diversity's need for greater aperture. Thus, the resolution lens

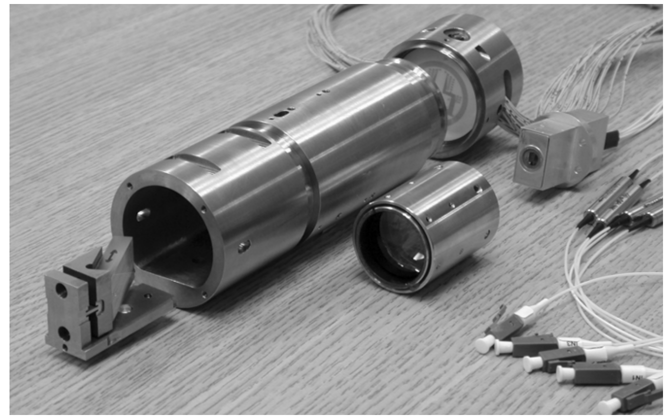

Fig. 10. Picture of components used to assemble 64-channel 4×1 wavelength-selective switch with spectral equalization. The 1100 lines/mm grating, the housing, the four-element 50 mm focal length resolution lens, the chip header, and the position to angle optical module are shown.

developed for the previous generation switch could be reused for the new five-fiber switch.

The MEMS micromirror arrays of the previous switch fulfilled the requirements of this switch and were both reused. The switch size and weight were the same as the previous generations, and shared all the SuperInvar parts. Optical isolators were placed on the four input fibers to prevent back reflections.

IV. Performance of Wavelength-Selective $1 \times K$ Switches

The three generations of our wavelength-selective switches were subjected to a sequence of tests for evaluating their performance. Spectral responses were obtained using an all-parameter test set.[1] Ten and forty Gb/s data rates using 33% RZ data modulation formats were used to test the channel passband effects on the 50-and 100-GHz based devices, respectively. The power penalty at an error rate of 10^{-9} was measured with a $2^{31} - 1$ PRBS error test set.

A. 128-Channel 1 × 4 Wavelength-Selective Switch

Our first-generation switch exhibited a 5-dB insertion loss value. However, it was possible to lower the loss figure to any one fiber to a much better value ($\sim$ 3 dB), at the expense of higher losses on the remaining output fibers. Polarization-dependent loss (PDL) was $\sim$ 1 dB, and reduced to 0.2 dB when optimizing to one particular port. The fiber-dependent loss and the relatively high PDL may be a consequence of system misalignment, lens aberrations, or grating image position dependence on output fiber when the micromirrors tilt in the dispersion direction.

The switch operated by setting the proper voltages to the electrodes in order to tilt the mirrors and switch to the desired output fibers (Fig. 11). The voltages for each mirror and output fiber power coupling were obtained by a simple "hill-climbing" training algorithm with one degree of freedom (mirror tilt, corresponding to driving voltage). The operating voltages were stored in a database and the established values did not drift significantly in our testing. This is due to the low voltage sensitivity when

[1] Agilent 81910A All Parameter Test System

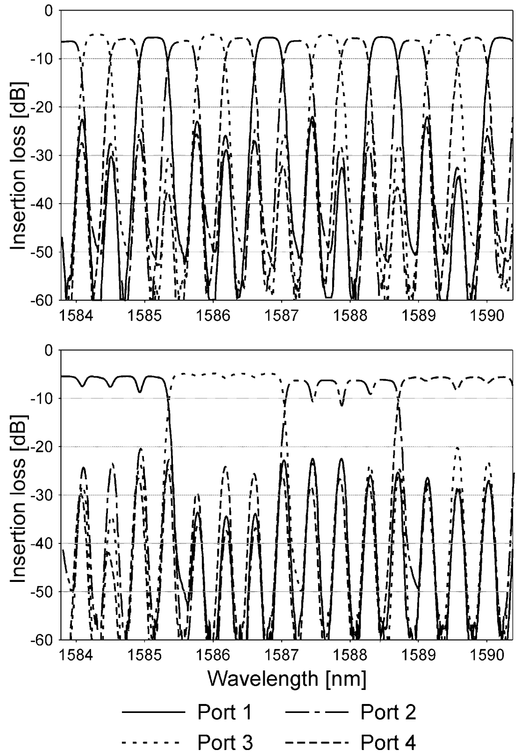

Fig. 11. Performance of 128-channel 1 $\times$ 4 wavelength-selective switch. Top frame: operation as a 4-port interleaver. Bottom frame: switching of bands to each port.

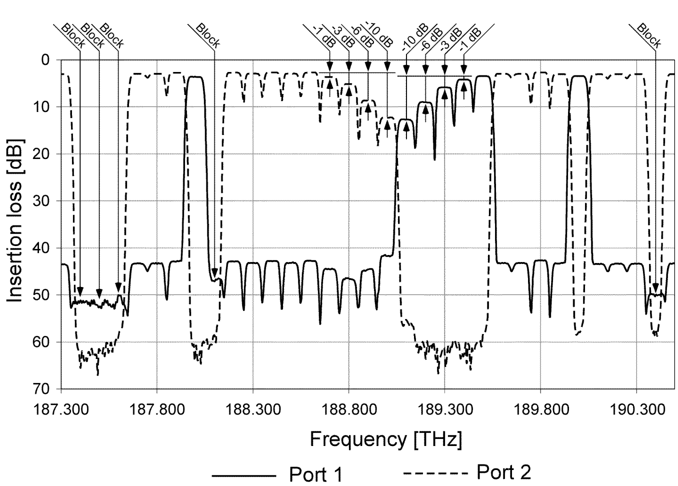

Fig. 12. Performance of 64-channel 1×2 wavelength-selective switch showing switching and spectral equalization. Spectral traces shows channels switching to either port 1 or 2, with attenuation settings up to 10 dB, as well as some blocked channels.

there are only four positions to address within the mirror tilt range, and the collimating lens apertures tightly pack the condenser lens aperture.

The observed power penalty for 10-Gb/s RZ data imposed by the channel passband was below -1 dB for laser center frequency detuning up to 15 GHz away from the channel's designated center frequency.

B. 64-Channel 1 $\times$ 2 Wavelength-Selective Switch With Spectral Equalization

The second-generation switch exhibited an improved insertion loss figure of 3 dB to output fiber 1 and 4 dB to output fiber 2 (Fig. 12). Part of the difference in loss between the output fibers is attributed to the double-passing of the circulator placed on the input/output fiber 2, as opposed to only a single pass when switching to output fiber 1. Having one fiber serve as both input and output also limited the directivity to 44 dB due to weak reflections from the connector at fiber 1 reaching output fiber 2. When switching directly back to the input fiber (or to output 2), the directivity is better than 60 dB.

The dynamic spectral equalization allowed attenuation values of up to 10 dB, while maintaining the directivity to better than 40 dB. Channel blocking was achieved by tilting a micromirror at a large angle, such that the reflected light is completely misaligned to the fibers. PDL was less than 0.3 dB, and differential group delay (DGD) was less than 0.4 ps, indicating that the polarization diversity is working as intended.

The observed power penalty for 40 Gb/s RZ data imposed by the channel passband was below -1.2 dB for laser center frequency detuning up to 25 GHz away from the channel's designated center frequency.

C. 64-Channel 4 $\times$ 1 Wavelength-Selective Switch With Spectral Equalization and Anamorphic Optics

The third-generation switch exhibited a worse-case insertion loss figure of 4 dB. This loss value includes the optical isolators placed on all the input fibers. Input fiber dependence still existed, with the input fiber farthest from the output fiber experiencing the highest loss.

This switch also supported the dynamic spectral equalization and channel blocking features (Fig. 13). Each of the four input fibers has an optimal voltage for coupling to the output fiber. Coupling loss was achieved by detuning from the ideal voltage such that the beam is shifted toward the gaps in the lens array (shaded zones in Fig. 13). As in the second generation switch, attenuation values of up to 10 dB were supported, while maintaining the directivity to better than 40 dB, and channel blocking was achieved by tilting the mirrors at large angles, such that the reflected light is completely misaligned to the output fibers.

Power penalty for 40-Gb/s data imposed by the channel passband was as good as for the 1 $\times$ 2 switch. PDL and DGD also did not deteriorate, as the anamorphic prism pair is placed after the implementation of the polarization diversity.

D. Channel Passband Comparison

The measured passband details of a single isolated channel for each switch version were superimposed for direct comparison, with the absolute insertion loss removed (Fig. 14). The measured frequency axis for each passband was also normalized with respect to the channel spacing, as our analysis has shown that the passband shape is determined primarily by the confinement factor (Section II-B).

Qualitatively, the passband curves match well with theory. As the confinement parameter ξ increases, the passband is flatter and wider, and with a sharper roll-off, resulting in a more box-

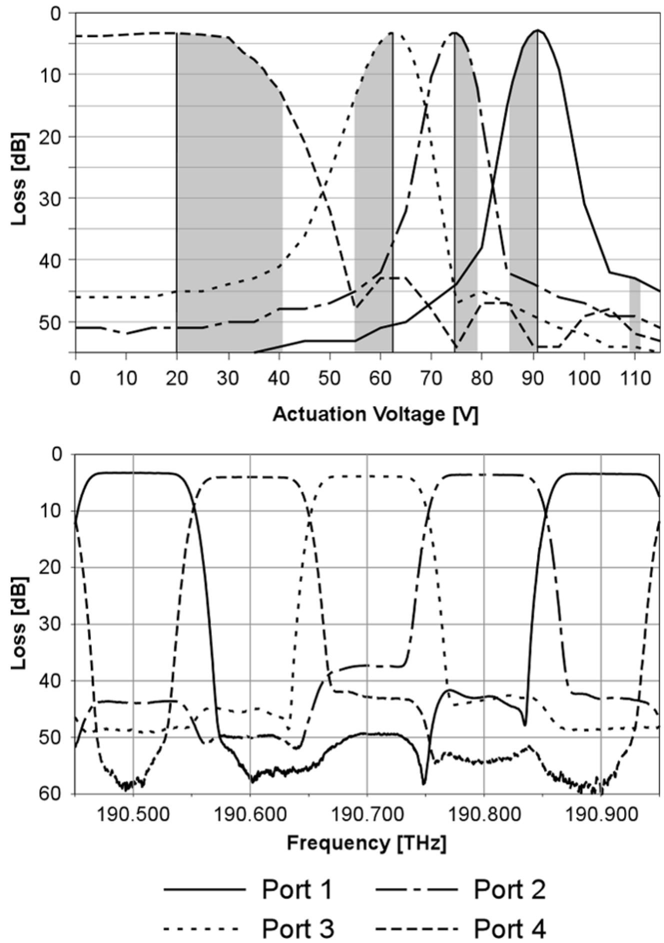

Fig. 13. Performance of 64-channel 4×1 wavelength-selective switch with spectral equalization and anamorphic optics. Top: Coupling from each input port and output port as a function of mirror actuation voltage. Shaded operating zones are used for attenuation settings from 0 to 10 dB. Bottom: Spectral traces of channels set in 4-port interleaver functionality.

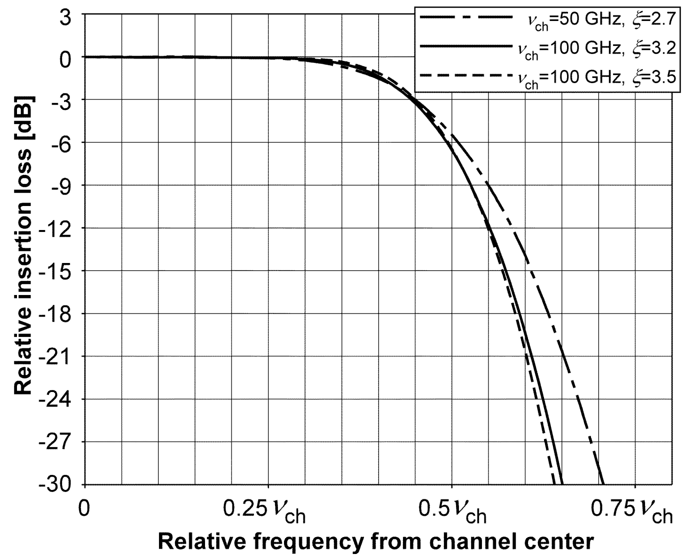

Fig. 14. Comparison of measured single-channel passbands for the switches presented. As the confinement factor increases, passband approaches ideal box shape. Frequency axis normalized by channel separation ν_{ch}.

like passband characteristics. The curves roughly intersect at the -3-dB-level, as opposed to the -6-dB-level in Fig. 5, due to the effect of the finite gap between adjacent mirrors slightly reducing the fill-factor in each implementation. The -1 dB-passband widths are used for comparing the passbands of the different switches. The -1 dB-passband of the 50 GHz, 1×4 switch was 37 GHz, or 0.74 of the channel spacing for $\xi = 2.7$. The 100-GHz, 1×2 switch, -1 dB-passband was 77 GHz (0.77 normalized for $\xi = 3.2$), and the 4×1 switch passband was 79 GHz (0.79 normalized for $\xi = 3.5$). The widening -1-dB normalized passband with increasing ξ highlights the significance of the confinement parameter in meeting the passband design requirements of the wavelength-selective switch. Similarly, the stopband width widens with increasing ξ, as evident from the intersection points of the curves at the -30-dB level in Fig. 14. The switch's pass- and block-band characteristics facilitates its use in optical mesh networking, limiting the amount of cascaded filtering and crosstalk a traversing signal would experience at intermediary nodes along the propagation path [27].

V. Conclusion

We have realized three generations of wavelength-selective $1 \times K$ switches, introducing new features in each generation. Our first-generation switch enabled the distribution of the input WDM channels across the K output fibers in a reconfigurable fashion. The second-generation switch incorporated dynamic spectral equalization at each output fiber, increasing the utility of the switch in optical networking. It also used a more robust tubular optomechanical housing construction. The third generation switch added anamorphic optics, assisting in minimizing the switch physical size.

The design parameters and system tradeoffs in implementing a wavelength-selective switch were described. The flexibility in choosing the magnification and anamorphic ratios of the imaging system in the first (magnifying) subassembly, and the amount of spatial dispersion and mirror-to-beam size ratio in the second (dispersing) subassembly enable us to provide wide and flat passbands for minimal signal distortion in a compact optical microsystem. The functionality and features provided by these switches make them desirable as WDM channel-switching elements in transparent networks.

References

[1] R. Ramaswami and K. Sivarajan, *Optical Networks: A Practical Perspective*. New York: Morgan Kaufmann, 1998.

[2] T. Stern and K. Bala, *Multiwavelength Optical Networks*. Reading, MA: Addison-Wesley, 1999.

[3] J. Ford, "Micromechanical wavelength add/drop switching: From device to network architecture," presented at the Optical Fiber Communication Conf., 2003.

[4] D. T. Neilson, D. S. Greywall, S. Chandrasekhar, L. L. Buhl, H. Tang, L. Ko, N. R. Basavanhally, F. Pardo, D. A. Ramsey, J. D. Weld, Y. L. Low, J. Prybyla, R. Scotti, A. Gasparyan, M. Haueis, S. Arney, S. P. O'Neill, C.-S. Pai, D. H. Malkani, M. M. Meyers, N. Saluzzi, S. H. Oh, O. D. Lopez, G. R. Bogart, F. P. Klemens, M. Luo, J. Q. Liu, K. Teffeau, A. Ramirez, K. S. Werder, J. E. Griffith, C. Frye, M. V. Kunnavakkam, S. T. Stanton, J. A. Liddle, H. T. Soh, T.-C. Lee, O. Nalamasu, and K. C. Nguyen, "High-dynamic range channelized MEMS equalizing filter," presented at the Optical Fiber Communication Conf., 2002, pp. 586–588.

[5] A. Boskovic, M. Sharma, N. Antoniades, and M. Lee, "Broadcast and select OADM nodes application and performance trade-offs," presented at the Optical Fiber Communication Conf., 2002, pp. 158–159.

[6] D. T. Neilson, H. Tang, D. S. Greywall, N. R. Basavanhally, L. Ko, D. A. Ramsey, J. D. Weld, Y. L. Low, F. Pardo, D. O. Lopez, P. Busch, J. Prybyla, M. Haueis, C. S. Pai, R. Scotti, and R. Ryf, "Channel equalization and blocking filter utilizing micro electro mechanical mirrors," IEEE J. Sel. Topics Quantum Electronics, vol. 10, no. 3, pp. 563–569, May./Jun.. 2004, to be published.

[7] J. E. Ford, V. A. Aksyuk, D. J. Bishop, and J. A. Walker, "Wavelength add-drop switching using tilting micromirrors," *J. Lightw. Technol.*, vol. 17, no. 5, pp. 904–911, May 1999.

[8] C. R. Doerr, L. W. Stulz, M. Cappuzzo, L. Gomez, A. Paunsecu, E. Laskowski, S. Chandrasekhar, and L. Buhl, "2 $\times$ 2 wavelength- selective cross connect capable of switching 128 channels in sets of eight," *IEEE Photon. Technol. Lett.*, vol. 14, no. 3, pp. 387–389, Mar. 2002.

[9] W. J. Tomlinson, "Dynamic gain equalization for next-generation DWDM transport systems," in *Advanced Semiconductor Lasers and Applications/Ultraviolet and Blue Lasers and Their Applications/Ultralong Haul DWDM Transmission and Networking/WDM Components, 2001 Dig. LEOS Summer Topical Meetings*, Jul.–Aug. 30–1, 2001, pp. 2–2.

[10] D. M. Marom, D. T. Neilson, D. S. Greywall, N. R. Basavanhally, P. R. Kolodner, Y. L. Low, C. A. Bolle, S. Chandrasekhar, L. Buhl, S.-H. Oh, C.-S. Pai, K. Werder, H. T. Soh, G. R. Bogart, E. Ferry, F. P. Klemens, K. Teffeau, J. F. Miner, S. Rogers, J. E. Bower, R. C. Keller, and W. Mansfield, "Wavelength selective 1 $\times$ 4 switch for 128 WDM channels at 50 GHz spacing," presented at the Optical Fiber Communication Conf., 2002, pp. 857–859.

[11] D. M. Marom, D. T. Neilson, D. S. Greywall, V. Aksyuk, M. E. Simon, N. R. Basavanhally, P. R. Kolodner, Y. L. Low, F. Pardo, C. A. Bolle, C. S. Pai, D. López, J. A. Taylor, J. E. Bower, J. Leuthold, M. Gibbons, and C. R. Giles, "Wavelength selective 4 $\times$ 1 switch with high spectral efficiency, 10 dB dynamic equalization range and internal blocking capability," in *ECOC*, Rimini, Italy, Sep. 21–25, 2003, Paper Mo3.5.3.

[12] T. Ducellier, J. Bismuth, S. F. Roux, A. Gillet, C. Merchant, M. Miller, M. Mala, Y. Ma, L. Tay, J. Sibille, M. Alavanja, A. Deren, M. Cugalj, D. Ivancevic, V. Dhuler, E. Hill, A. Cowen, B. Shen, and R. Wood, "The MWS 1 $\times$ 4: A high performance wavelength switching building block," presented at the ECOC, 2002.

[13] M. C. Wu, J. C. Tsai, S. Huang, and H. Dooyoung, "MEMS WDM routers using analog micromirror arrays," in *Lasers and Electro-Optics Society, 2002. LEOS 2002. The 15th Ann. Meeting IEEE*, vol. 2, Nov. 10–14, 2002, pp. 582–583.

[14] D. T. Fuchs, C. R. Doerr, V. A. Aksyuk, M. E. Simon, L. W. Stulz, S. Chandrasekhar, L. L. Buhl, M. Cappuzzo, L. Gomez, A. Wong-Foy, E. Laskowski, E. Chen, and R. Pafchek, "A hybrid MEMS-waveguide wavelength selective cross connect," *IEEE Photon. Technol. Lett.*, vol. 16, no. 1, pp. 99–101, Jan. 2004.

[15] C. R. Doerr, L. W. Stulz, D. S. Levy, L. Gomez, M. Cappuzzo, J. Bailey, R. Long, A. Wong-Foy, E. Laskowski, E. Chen, S. Patel, and T. Murphy, "Eight-wavelength add-drop filter with true reconfigurability," *IEEE Photon. Technol. Lett.*, vol. 15, no. 1, pp. 138–140, Jan. 2003.

[16] D. M. Marom, D. T. Neilson, J. Leuthold, M. Gibbons, and C. R. Giles, "64 channel 4 $\times$ 4 wavelength-selective cross-connect for 40 Gb/s channel rates with 10 Tb/s throughput capacity," in *ECOC*, Rimini, Italy, Sep. 21–25, 2003, Paper We4.P.130.

[17] M. Vasilyev, I. Tomkos, M. Mehendale, J.-K. Rhee, A. Kobyakov, M. Ajgaonkar, S. Tsuda, and M. Sharma, "Transparent ultra-long-haul DWDM networks with "broadcast-and-select" OADM/OXC architecture," *J. Lightw. Technol.*, vol. 21, no. 11, pp. 2661–2672, Nov. 2003.

[18] J. E. Ford, D. J. DiGiovanni, and D. J. Reiley, "1 $\times$ N fiber bundle scanning switch," in *Optical Fiber Communication Conf. '98, Tech. Dig.*, Feb. 22–27, 1998, pp. 143–144.

[19] R. E. Wagner and W. J. Tomlinson, "Coupling efficiency of optics in single-mode fiber components," *Appl. Opt.*, vol. 21, pp. 2671–2688, 1982.

[20] E. G. Loewen and E. Popov, *Diffraction Gratings and Application*. New York: Marcel Dekker, 1997.

[21] D. M. Marom and S. Oh, "Filter-shape dependence on attenuation mechanism in channelized dynamic spectral equalizers," in *15th Ann. Meeting Lasers Electro-Optics Society, 2002. LEOS 2002*, vol. 2, Nov. 13–14, 2002, pp. 416–417.

[22] D. M. Marom, D. T. Neilson, R. Ryf, and H. Shea, "Effect of mirror curvature in MEMS micro-mirror based wavelength-selective switches," in *LEOS 16th Annu. Meeting 2003*, Tucson, AZ, paper TuO4.

[23] S. Pau, N. Chand, K. Kojima, and V. Swaminathan, "Transient effects and cascadability of an MEMS-based dynamic-gain equalizing filter: A case study," *IEEE Photon. Technol. Lett.*, vol. 15, no. 2, pp. 347–349, Feb. 2003.

[24] "Model 54-∗-544H," Richardson Grating Laboratory (now Spectra Physics).

[25] D. López, M. E. Simon, F. Pardo, V. Aksyuk, F. Klemens, R. Cirelli, D. T. Neilson, H. Shea, T. Sorsch, E. Ferry, O. Nalamasu, and P. L. Gammel, "Monolithic MEMS optical switch with amplified out-of-plane angular motion," in *MOEMS 2002 Int. Conf. Optical MEMS*, Lugano, Switzerland, Aug. 2002, Paper ThB5, pp. 165–166.

[26] D. S. Greywall, C.-S. Pai, S. H. Oh, C.-P. Chang, D. M. Marom, P. A. Busch, R. A. Cirelli, J. A. Taylor, F. P. Klemens, T. W. Sorsch, J. E. Bower, W. Y.-C. Lai, and H. T. Soh, "Monolithic, fringe-field-activated crystaline silicon tilting mirror devices," *J. Microelectromechanical Syst.*.

[27] H. K. Kim, S. Chandrasekhar, M. Spector, and L. Buhl, "Error-free operation of a large scale (16 nides cascaded over total distance of 600 km) optical network based on dense WDM (15 100 GHz-spaced 10 Gbit/s/channel) channels," *Elec. Lett.*, vol. 36, pp. 654–655, 2000.

Dan M. Marom (M'99) received the B.Sc. degree in mechanical engineering and the M.Sc. degree in electrical engineering, both from Tel-Aviv University, Tel-Aviv, Israel, in 1989 and 1995, respectively, and the Ph.D. from the University of California, San Diego, in 2000. In his doctoral dissertation he investigated femtosecond-rate optical signal processing with applications in ultrafast communications.

From 1996 through 2000, he was a Fannie and John Hertz Foundation Graduate Fellow at UCSD. In 2000, he joined the Advanced Photonics Research Department at Bell Laboratories, Lucent Technologies, Holmdel, NJ, where he is working on novel MEMS-based switching solutions using MEMS technology for optical communications.

Dr. Marom received the IEEE Lasers and Electro-Optics Society best student paper award in 1999 for his work describing instantaneous time reversal of complex amplitude ultrafast waveforms.

David T. Neilson (M'96–SM'02) received the B.Sc. (Hons) degree in physics from Heriot-Watt University, Edinburgh, Scotland, in 1990 and the Ph.D. degree in physics for work on optical nonlinearities in InGaAs Quantum well devices from Heriot-Watt University in 1993.

He was a Postdoctoral Researcher at Heriot-Watt University from 1993 to 1996, working on systems and devices for free space optical interconnects. From 1996 to 1998, he was a Visiting Scientist at NEC Research Institute, Princeton, NJ, researching optical interconnects for high-performance computing. In 1998, he joined Bell Laboratories, Holmdel, NJ, where he has worked on MEMS-based crossconnects, wavelength selective switches, equalizers, and dispersion compensators. He is currently a Technical Manager with responsibility for optoelectronic device growth and fabrication facility. He has over 80 publications in the field of optical interconnects and switching.

Dr. Neilson is a Senior Member of LEOS and a Member of the Optical Society of America (OSA).

Dennis S. Greywall received the B.S. degree in physics from the University of Detroit, Detroit, MI, in 1965 and the Ph.D. degree in low-temperature physics from Indiana University in 1970.

Immediately thereafter, he joined Bell Laboratories, Murray Hill, NJ, where he is a Distinguished Member of Technical Staff. His work has included experimental studies of helium crystals, superfluidity in 3He and 4He, and magnetism in two-dimensional 3He. He has also worked on noise evasion and on mechanical dissipation in very small systems at very low temperatures. Since 1995, his focus has been on the mechanical design and modeling of MOEMS devices such as modulators, cross connects, and wavelength sorting switches. In addition, he has designed microelectromechanical systems (MEMS)-based radio frequency filters, *in vivo* medical devices, and adaptive optics mirrors.

Dr. Greywall is a Fellow of the American Physical Society and was the recipient of the 1993 London Prize in Low Temperature Physics.

Chien-Shing Pai received the B.S. degree in electrophysics from Chiao-Tung University, Hsin-Chu, Taiwan, R.O.C., in 1978 and the Ph.D. degree in electrical engineering from the University of California, San Diego, in 1985.

Since 1985, he worked at Bell Laboratories, Murray Hill, NJ, in the area of Advanced Electronic Device Research, where he is now a Distinguished Member of Technical Staff. He was involved in the research and development in both device and processing for advanced complementary metal–oxide–semiconductor (CMOS) technologies for ULSI applications. His work included selective-epi and silicide for front-end CMOS device and low-k materials and multilevel-interconnect integration for sub-100 nm ULSI applications. Since 2000, his work expanded to include microelectromechanical systems (MEMS) technology for communication and biotech applications.

Dr. Pai served as a Committee Member in VLSI Technology Symposium since 1996 and has organized and chaired short course and rump session for several years.

Nagesh R. Basavanhally photograph and biography not available at the time of publication.

Vladimir A. Aksyuk, photograph and biography not available at the time of publication.

Daniel O. López, photograph and biography not available at the time of publication.

Flavio Pardo, photograph and biography not available at the time of publication.

Maria Elina Simon, photograph and biography not available at the time of publication.

Yee Low, photograph and biography not available at the time of publication.

Paul Kolodner received the A.B. degree in physics from Princeton University, Princeton, NJ, in 1975 and the A.M. and Ph.D. degrees in physics from Harvard University, Cambridge, MA, in 1977 and 1980, respectively. His Ph.D. work was on suprathermal electron emission produced by laser-induced breakdown of fast shockfronts.

Since 1980, he has worked at Bell Laboratories, Murray Hill, NJ, on a variety of experimental problems, including the use of rare-earth-chelate films for high-resolution fluorescent thermal imaging, pattern formation in binary-fluid convection, photobiology of bacteriorhodopsin, and applications of superhydrophobic surfaces in drag reduction and thermal management. He has written or coauthored approximately 90 published papers and has 13 issued or pending patents. He is presently a Distinguished Member of Technical Staff in the Network Hardware Integration Department of Bell Laboratories.

Cristian A. Bolle was born in Buenos Aires, Argentina, in 1966. He received the M.S. and Ph.D. in physics from the Instituto Balseiro, Argentina, in 1990 and 1995, respectively. In 1997, he joined the Microsystems Research Group in Lucent Technologies Bell Laboratories, Murray Hill, NJ, where he worked in the research of mesoscopic superconductors at low temperatures as well as the development of the Lambda router all optical switch. He has also be engaged in thermal management and cost reduction activities closely related to Lucent products.

Dr. Bolle is a Member of the American Physical Society.